

# THREE-DIMENSIONAL SIMULATIONS OF A CONSERVED BINARY MIXTURE USING MODEL B

Rudimar Luiz Nos<sup>1\*</sup>, Hector Daniel Cenicer<sup>2</sup> and Alexandre Megiorin  
Roma<sup>3</sup>

1: Department of Mathematics  
UTFPR - Federal University of Technology - Paraná  
Avenida Sete de Setembro, 3165 80230-901 Curitiba, PR, Brazil  
e-mail: rudimarnos@utfpr.edu.br, web: <http://paginapessoal.utfpr.edu.br/rudimarnos>

2: Department of Mathematics  
UCSB - University of California at Santa Barbara  
South Hall 6710 93106 Santa Barbara, CA, USA  
e-mail: hdc@math.ucsb.edu, web: <http://math.ucsb.edu/~hdc>

3: Department of Applied Mathematics  
USP - University of São Paulo  
Rua do Matão, 1010 05508-090 São Paulo, SP, Brazil  
e-mail: roma@ime.usp.br, web: <http://www.ime.usp.br/~roma>

**Keywords:** Cahn-Hilliard equation, Model B, Planar and homeotropic anchoring, Multilevel multigrid, Semi-implicit methods, Nematic liquid crystal

**Abstract.** *We present three-dimensional numerical simulations of a binary mixture with a nematic liquid crystal and flexible polymer phases. The model is based on the Ginzburg-Landau free energy and is defined by coupling the Cahn-Hilliard equation, which incorporates the nematic elastic energy and guide spinodal decomposition, with the de Gennes-Prost equation, which governs the crystal's director field. The main goal is to analyze how the orientational distortion of the director field induced by interfacial anchoring affects both the morphology and the ordering kinetics of the binary mixture in three dimensions.*

## 1 INTRODUCTION

This work is a part of the research carried out by first author during his post-doctorate at UCSB<sup>1</sup>. It is a continuation of the work already presented by the authors [1] [2] [3] [4] and it is also a three-dimensional extension of the work developed by [5].

Binary alloys and polymer blends have been extensively studied [6] [7] and systems in which one of the components is a liquid crystal are receiving more attention [8] [9] [10] [11]

---

<sup>1</sup>This research has been funded by Capes.

[12] [13]. In this work we simulate numerically the phase separation kinetics of a three-dimensional binary system in which one of the components is a nematic<sup>2</sup> liquid crystal and the other component is a flexible polymer with Ginzburg-Landau free energy [14]. The system is modeled through an order parameter or phase field  $\phi$ , which is a measure of the volume fraction of one of the components, and a director field  $\mathbf{n}$ , which quantifies the mean orientational order in the nematic liquid crystal phase. This model is called Model B according to the nomenclature of Hohenberg and Halperin [15] and its dynamics are driven by energy minimization with conserved  $\phi$ . Particularly, the model that we employ differs from that considered by [16] because we keep both elastic and anchoring terms in the Cahn-Hilliard equation.

## 2 MATHEMATICAL MODEL

Model B can be described with a phase field  $\phi$  related to the species concentration and with the director field  $\mathbf{n}$ , which is a measure of the mean molecular orientation in the nematic liquid crystal phase. Specifically,  $(1 + \phi)/2$  represents the nematic phase concentration and  $(1 - \phi)/2$  the flexible polymer component concentration.

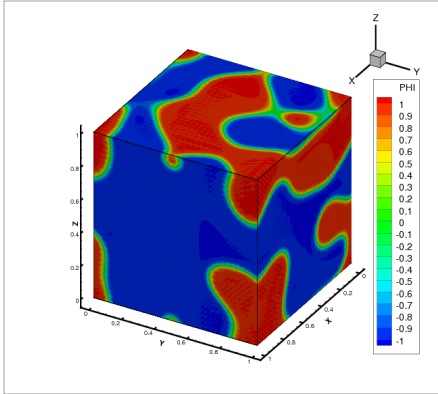


Figure 1: Components of the binary mixture: nematic liquid crystal ( $\phi = 1$ ), in red, and flexible polymer ( $\phi = -1$ ), in blue.

The pure, bulk phases are identified with  $\phi = 1$  and  $\phi = -1$  for the nematic liquid crystal and the flexible polymer component, respectively. A narrow neighborhood of the level set  $\phi = 0$  provides a diffuse interface between the two species, as shown in Figure 1.

The free energy of the system consists of three parts: a mixing energy  $f_{\text{mix}}$ , a bulk, orientational distortion energy of the nematic,  $f_{\text{bulk}}$ , and the anchoring energy of the liquid crystal molecules on the interface,  $f_{\text{anch}}$  [16], being given by

$$f(\phi, \mathbf{n}) = f_{\text{mix}} + \frac{1 + \phi}{2} f_{\text{bulk}} + f_{\text{anch}}, \quad (1)$$

where

$$f_{\text{mix}} = \frac{\lambda}{2} \left[ |\nabla \phi|^2 + \frac{(\phi^2 - 1)^2}{2\epsilon^2} \right], \quad (2)$$

<sup>2</sup>Relating to or denoting a state of a liquid crystal in which the molecules are oriented in parallel but not arranged in well-defined planes.

$$f_{\text{bulk}} = \frac{K}{2} \left[ \nabla \mathbf{n} : (\nabla \mathbf{n})^T + \frac{(|\mathbf{n}|^2 - 1)^2}{2\delta^2} \right], \quad (3)$$

$$f_{\text{anch}} = \begin{cases} \frac{A}{2} (\mathbf{n} \cdot \nabla \phi)^2 & \text{(planar anchoring),} \\ \frac{A}{2} [|\mathbf{n}|^2 |\nabla \phi|^2 - (\mathbf{n} \cdot \nabla \phi)^2] & \text{(homeotropic anchoring).} \end{cases} \quad (4)$$

In (2),  $\lambda$  is the mixing energy density and  $\varepsilon$  is the capillary width. Equation (3) is the regularized Frank energy in which the elastic constants for splay, twist, and bend are all equal to  $K$  and  $(|\mathbf{n}| - 1)^2/(2\delta^2)$  is a penalty term to approximately enforce the constraint  $|\mathbf{n}| = 1$ . Finally, in (4),  $A$  is the strength of the anchoring. The planar anchoring energy density favors alignment of the director tangential to the interface whereas for the homeotropic anchoring the alignment of  $\mathbf{n}$  is perpendicular to it.

The corresponding Cahn-Hilliard equation [17] [18] governing the dynamics of the order parameter is

$$\frac{\partial \phi}{\partial t} = \nabla \cdot [\gamma \nabla \mu], \quad (5)$$

where

$$\mu = \frac{\delta F}{\delta \phi} \quad (6)$$

is the chemical potential,

$$F = \int_{\Omega} f(\phi, \mathbf{n}, \nabla \phi, \nabla \mathbf{n}) dx \quad (7)$$

is the total free energy,  $\Omega$  is the region of space occupied by the system and  $\gamma$  is the mobility, which in this work it is assumed to be a constant. Taking all the contributions to the energy, (2)-(4), we have

$$\mu = \lambda \left[ -\nabla^2 \phi + \frac{\phi(\phi^2 - 1)}{\varepsilon^2} \right] + \frac{K}{4} \left[ \nabla \mathbf{n} : (\nabla \mathbf{n})^T + \frac{(|\mathbf{n}|^2 - 1)^2}{2\delta^2} \right] + \mu_{\text{anch}}, \quad (8)$$

where

$$\mu_{\text{anch}} = \begin{cases} -A \nabla \cdot [(\mathbf{n} \cdot \nabla \phi) \mathbf{n}] & \text{(planar anchoring),} \\ -A \nabla \cdot [|\mathbf{n}|^2 \nabla \phi - (\mathbf{n} \cdot \nabla \phi) \mathbf{n}] & \text{(homeotropic anchoring).} \end{cases} \quad (9)$$

The director evolves following the simplified Leslie-Ericksen theory due to de Gennes and Prost [19]

$$\frac{1}{\tau} \frac{\partial \mathbf{n}}{\partial t} = -\frac{\delta F}{\delta \mathbf{n}} \quad (10)$$

and is used by Yue, Feng, Liu, and Shen [16], where  $\tau$  is a measure of the relaxation time of the director. Then the coupled system of equations governing the phase separation of the mixture is

$$\begin{aligned} \frac{\partial \phi}{\partial t} = & \gamma \nabla^2 \left[ \lambda \left( -\nabla^2 \phi + \frac{\phi^3 - \phi}{\varepsilon^2} \right) + \right. \\ & \left. + \frac{K}{4} \left( \nabla \mathbf{n} : (\nabla \mathbf{n})^T + \frac{(|\mathbf{n}|^2 - 1)^2}{2\delta^2} \right) + \mu_{\text{anch}} \right], \end{aligned} \quad (11)$$

$$\frac{1}{\tau} \frac{\partial \mathbf{n}}{\partial t} = K \left[ \nabla \cdot \left( \frac{1 + \phi}{2} \nabla \mathbf{n} \right) - \frac{1 + \phi}{2} \frac{(|\mathbf{n}|^2 - 1)\mathbf{n}}{\delta^2} \right] - \mathbf{g}, \quad (12)$$

where  $\mu_{\text{anch}}$  is given by (9) and

$$\mathbf{g} = \begin{cases} A(\mathbf{n} \cdot \nabla \phi) \nabla \phi & \text{(planar anchoring),} \\ A[|\nabla \phi|^2 \mathbf{n} - (\mathbf{n} \cdot \nabla \phi) \nabla \phi] & \text{(homeotropic anchoring).} \end{cases} \quad (13)$$

To define the semi-implicit scheme, a term is added and subtracted in the equations (11) and (12). As mobility  $\lambda$  is constant, the system (11)-(12) can be rewritten as

$$\begin{aligned} \frac{\partial \phi}{\partial t} = & \gamma \lambda \nabla^2 \left( \frac{\alpha}{\varepsilon^2} \phi - \nabla^2 \phi \right) + \\ & + \gamma \nabla^2 \left[ \frac{\lambda}{\varepsilon^2} (\phi^3 - \phi) + \frac{K}{4} \left( \nabla \mathbf{n} : (\nabla \mathbf{n})^T + \frac{(|\mathbf{n}|^2 - 1)^2}{2\delta^2} \right) + \mu_{\text{anch}} \right] + \\ & - \gamma \lambda \frac{\alpha}{\varepsilon^2} \nabla^2 \phi, \end{aligned} \quad (14)$$

$$\begin{aligned} \frac{\partial \mathbf{n}}{\partial t} = & \tau K \beta \nabla^2 \mathbf{n} + \\ & + \tau K \left[ \nabla \cdot \left( \frac{1 + \phi}{2} \nabla \mathbf{n} \right) - \frac{1 + \phi}{2} \frac{(|\mathbf{n}|^2 - 1)\mathbf{n}}{\delta^2} \right] - \tau \mathbf{g} + \\ & - \tau K \beta \nabla^2 \mathbf{n}. \end{aligned} \quad (15)$$

To avoid the direct discretization of the biharmonic term and to employ a linear multigrid, equation (14) is rewritten as a system of two equations using the replacements

$$\phi_1 = \phi \quad (16)$$

and

$$\phi_2 = \frac{\alpha}{\varepsilon^2} \phi_1 - \nabla^2 \phi_1. \quad (17)$$

Thus, the system (14)-(15) is rewritten as

$$\begin{aligned} \frac{\partial \phi_1}{\partial t} = & \gamma \lambda \nabla^2 \phi_2 + \\ & + \gamma \nabla^2 \left[ \frac{\lambda}{\varepsilon^2} (\phi_1^3 - \phi_1) + \frac{K}{4} \left( \nabla \mathbf{n} : (\nabla \mathbf{n})^T + \frac{(|\mathbf{n}|^2 - 1)^2}{2\delta^2} \right) + \mu_{\text{anch}} \right] + \\ & - \gamma \lambda \frac{\alpha}{\varepsilon^2} \nabla^2 \phi_1, \end{aligned} \quad (18)$$

$$\phi_2 = \frac{\alpha}{\varepsilon^2} \phi_1 - \nabla^2 \phi_1, \quad (19)$$

$$\begin{aligned} \frac{\partial \mathbf{n}}{\partial t} = & \tau K \beta \nabla^2 \mathbf{n} + \\ & + \tau K \left[ \nabla \cdot \left( \frac{1 + \phi_1}{2} \nabla \mathbf{n} \right) - \frac{1 + \phi_1}{2} \frac{(|\mathbf{n}|^2 - 1) \mathbf{n}}{\delta^2} \right] - \tau \mathbf{g} + \\ & - \tau K \beta \nabla^2 \mathbf{n}, \end{aligned} \quad (20)$$

where  $\mu_{\text{anch}}$  is given by

$$\mu_{\text{anch}} = \begin{cases} -A \nabla \cdot [(\mathbf{n} \cdot \nabla \phi_1) \mathbf{n}] & \text{(planar anchoring),} \\ -A \nabla \cdot [|\mathbf{n}|^2 \nabla \phi_1 - (\mathbf{n} \cdot \nabla \phi_1) \mathbf{n}] & \text{(homeotropic anchoring),} \end{cases} \quad (21)$$

and  $\mathbf{g}$  by

$$\mathbf{g} = \begin{cases} A(\mathbf{n} \cdot \nabla \phi_1) \nabla \phi_1 & \text{(planar anchoring),} \\ A[|\nabla \phi_1|^2 \mathbf{n} - (\mathbf{n} \cdot \nabla \phi_1) \nabla \phi_1] & \text{(homeotropic anchoring).} \end{cases} \quad (22)$$

### 3 NUMERICAL METHODOLOGY

The numerical scheme is a linearly implicit discretization, as the one considered in [20] and [3], in which the implicit part is discretized using a second-order backward difference formula (BDF) and the explicit part corresponds to a second order Adams-Bashforth method. The scheme can be written as

$$\frac{\frac{3}{2}\phi_1^{n+1} - 2\phi_1^n + \frac{1}{2}\phi_1^{n-1}}{\Delta t} = \gamma \lambda \nabla^2 \phi_2^{n+1} + 2\mathcal{F}(\phi_1^n, \phi_2^n, \mathbf{n}^n) - \mathcal{F}(\phi_1^{n-1}, \phi_2^{n-1}, \mathbf{n}^{n-1}), \quad (23)$$

$$\phi_2^{n+1} = \frac{\alpha}{\varepsilon^2} \phi_1^{n+1} - \nabla^2 \phi_1^{n+1}, \quad (24)$$

$$\frac{\frac{3}{2}\mathbf{n}^{n+1} - 2\mathbf{n}^n + \frac{1}{2}\mathbf{n}^{n-1}}{\Delta t} = \tau K \beta \nabla^2 \mathbf{n}^{n+1} + 2\mathcal{G}(\phi_1^n, \mathbf{n}^n) - \mathcal{G}(\phi_1^{n-1}, \mathbf{n}^{n-1}), \quad (25)$$

where

$$\mathcal{F}(\phi_1, \phi_2, \mathbf{n}) = \gamma \nabla^2 \left[ \frac{\lambda}{\varepsilon^2} (\phi_1^3 - \phi_1) + \frac{K}{4} \left( \nabla \mathbf{n} : (\nabla \mathbf{n})^T + \frac{(|\mathbf{n}|^2 - 1)^2}{2\delta^2} \right) + \mu_{\text{anch}} \right] - \gamma \lambda \frac{\alpha}{\varepsilon^2} \left( \frac{\alpha}{\varepsilon^2} \phi_1 - \phi_2 \right), \quad (26)$$

$$\mathcal{G}(\phi_1, \mathbf{n}) = \tau K \left[ \nabla \cdot \left( \frac{1 + \phi_1}{2} \nabla \mathbf{n} \right) - \frac{1 + \phi_1}{2} \frac{(|\mathbf{n}|^2 - 1) \mathbf{n}}{\delta^2} \right] - \tau \mathbf{g} + \tau K \beta \nabla^2 \mathbf{n}, \quad (27)$$

and  $\mu_{\text{anch}}$  is given by

$$\mu_{\text{anch}} = \begin{cases} -A \nabla \cdot [(\mathbf{n} \cdot \nabla \phi_1) \mathbf{n}] & \text{(planar anchoring),} \\ -A \nabla \cdot [|\mathbf{n}|^2 \nabla \phi_1 - (\mathbf{n} \cdot \nabla \phi_1) \mathbf{n}] & \text{(homeotropic anchoring),} \end{cases} \quad (28)$$

and  $\mathbf{g}$  by

$$\mathbf{g} = \begin{cases} A(\mathbf{n} \cdot \nabla \phi_1) \nabla \phi_1 & \text{(planar anchoring),} \\ A[|\nabla \phi_1|^2 \mathbf{n} - (\mathbf{n} \cdot \nabla \phi_1) \nabla \phi_1] & \text{(homeotropic anchoring).} \end{cases} \quad (29)$$

Here,  $\alpha$  and  $\beta$  are numerical parameters to relax the time step stability constraint [20]. In the simulations reported in this work we take  $\alpha = 2$  and  $\beta = 1$ . In addition, to limit the terms  $(1 + \phi)/2$  from exceeding 1 due to numerical overshoot, we approximate this term by  $(1 + s\phi)/2$ , where  $s = 0.90$ . These equations are solved on a cube  $[0, 2] \times [0, 2] \times [0, 2]$  with periodic boundary conditions. The spatial derivatives are discretized with standard second order finite differences on a uniform grid  $256 \times 256 \times 256$  and linear systems arising from the discretization are solved through the multigrid [2] [3] [4]. The time step  $\Delta t$  used is equal to  $10^{-1}$  and spatial step  $h = \Delta x = \Delta y = \Delta z$  is equal to  $\frac{2}{256}$ .

#### 4 ACCURACY TEST

We validate the proposed numerical approach in the unit cube using uniform grids. The purpose of this test is to verify that the errors introduced by interpolation and discretization schemes are correctly controlled to prevent global accuracy degradation.

For this test, we construct an exact solution  $(\phi_e, \mathbf{n}_e)$  to the following forced Model H equations:

$$\begin{aligned} \frac{\partial \phi_1}{\partial t} &= \gamma \lambda \nabla^2 \phi_2 + \\ &+ \gamma \nabla^2 \left[ \frac{\lambda}{\varepsilon^2} (\phi_1^3 - \phi_1) + \frac{K}{4} \left( \nabla \mathbf{n} : (\nabla \mathbf{n})^T + \frac{(|\mathbf{n}|^2 - 1)^2}{2\delta^2} \right) + \mu_{\text{anch}} \right] + \\ &- \gamma \lambda \frac{\alpha}{\varepsilon^2} \nabla^2 \phi_1 + F_{\text{CH}}(\phi_{1e}, \phi_{2e}, \mathbf{n}_e), \end{aligned} \quad (30)$$

$$\phi_2 = \frac{\alpha}{\varepsilon^2} \phi_1 - \nabla^2 \phi_1, \quad (31)$$

$$\begin{aligned} \frac{\partial \mathbf{n}}{\partial t} = & \tau K \beta \nabla^2 \mathbf{n} + \\ & + \tau K \left[ \nabla \cdot \left( \frac{1 + \phi_1}{2} \nabla \mathbf{n} \right) - \frac{1 + \phi_1}{2} \frac{(|\mathbf{n}|^2 - 1) \mathbf{n}}{\delta^2} \right] - \tau \mathbf{g} + \\ & - \tau K \beta \nabla^2 \mathbf{n} + \mathbf{F}_{\text{VD}}(\phi_{1e}, \mathbf{n}_e), \end{aligned} \quad (32)$$

where  $\mu_{\text{anch}}$  is given by

$$\mu_{\text{anch}} = -A \nabla \cdot [(\mathbf{n} \cdot \nabla \phi_1) \mathbf{n}] \quad (\text{planar anchoring}), \quad (33)$$

and  $g$  by

$$\mathbf{g} = A(\mathbf{n} \cdot \nabla \phi_1) \nabla \phi_1 \quad (\text{planar anchoring}). \quad (34)$$

Naturally, in (30) and (32),

$$\begin{aligned} F_{\text{CH}}(\phi_{1e}, \phi_{2e}, \mathbf{n}_e) = & \frac{\partial \phi_{1e}}{\partial t} - \gamma \lambda \nabla^2 \phi_{2e} - \gamma \nabla^2 \left[ \frac{\lambda}{\varepsilon^2} (\phi_{1e}^3 - \phi_{1e}) + \right. \\ & + \frac{K}{4} \left( \nabla \mathbf{n}_e : (\nabla \mathbf{n}_e)^T + \frac{(|\mathbf{n}_e|^2 - 1)^2}{2\delta^2} \right) + \mu_{\text{anch}_e} \left. \right] + \\ & + \gamma \lambda \frac{\alpha}{\varepsilon^2} \left( \frac{\alpha}{\varepsilon^2} \phi_{1e} - \phi_{2e} \right), \end{aligned} \quad (35)$$

$$\begin{aligned} \mathbf{F}_{\text{VD}}(\phi_{1e}, \mathbf{n}_e) = & \frac{\partial \mathbf{n}_e}{\partial t} - \tau K \beta \nabla^2 \mathbf{n}_e + \\ & - \tau K \left[ \nabla \cdot \left( \frac{1 + \phi_{1e}}{2} \nabla \mathbf{n}_e \right) - \frac{1 + \phi_{1e}}{2} \frac{(|\mathbf{n}_e|^2 - 1) \mathbf{n}_e}{\delta^2} \right] + \\ & + \tau \mathbf{g}_e + \tau K \beta \nabla^2 \mathbf{n}_e, \end{aligned} \quad (36)$$

and  $\phi_1(0, \mathbf{x}) = \phi_{1e}(0, \mathbf{x})$ , and  $\phi_2(0, \mathbf{x}) = \phi_{2e}(0, \mathbf{x})$ , and  $\mathbf{n}(0, \mathbf{x}) = \mathbf{n}_e(0, \mathbf{x})$ .

We select  $(\phi_{1e}, \mathbf{n}_e = (n_{xe}, n_{ye}, n_{ze}))$  as follows:

$$\phi_{1e}(t, \mathbf{x}) = \sin^3(2\pi(x + y + z + t)), \quad (37)$$

$$n_{xe}(t, \mathbf{x}) = 0, \quad (38)$$

$$n_{ye}(t, \mathbf{x}) = \cos(2\pi(x + y + z + t)), \quad (39)$$

$$n_{ze}(t, \mathbf{x}) = \sin(2\pi(x + y + z + t)). \quad (40)$$

The equations (30)-(34) were solved in the unit cube  $\Omega = [0, 1] \times [0, 1] \times [0, 1]$  with periodic boundary conditions and  $0 < t \leq 10$ ,  $\alpha = 2$ ,  $\beta = 1$ ,  $\varepsilon = 0.125$ ,  $\gamma = 0.00001$ ,  $\tau = 0.5$ ,  $\lambda = 0.1$ ,  $\delta = 0.5$ , and  $K = A = 0.006708$ .

Table 1 show the errors and convergence ratios for this case. The convergence ratios indicate that the error appears to be consistent with that of a second order discretization [1] [2] [3] [4] [21].

$n$	Variable	Norm	$R$
32	$\phi$	$\ \phi - \phi_e\ _2 = 2.269320008828050 \times 10^{-2}$	
	$n_x$	$\ n_x - n_{xe}\ _2 = 1.649338034918546 \times 10^{-3}$	
	$n_y$	$\ n_y - n_{ye}\ _2 = 1.038634062541942 \times 10^{-2}$	
	$n_z$	$\ n_z - n_{ze}\ _2 = 1.078656325408673 \times 10^{-2}$	
64	$\phi$	$\ \phi - \phi_e\ _2 = 6.059074243078967 \times 10^{-3}$	3.75
	$n_x$	$\ n_x - n_{xe}\ _2 = 5.154721285378072 \times 10^{-4}$	3.20
	$n_y$	$\ n_y - n_{ye}\ _2 = 2.784391310165071 \times 10^{-3}$	3.73
	$n_z$	$\ n_z - n_{ze}\ _2 = 2.659065270324107 \times 10^{-3}$	4.06
128	$\phi$	$\ \phi - \phi_e\ _2 = 1.545196350195382 \times 10^{-3}$	3.92
	$n_x$	$\ n_x - n_{xe}\ _2 = 1.400611891955155 \times 10^{-4}$	3.68
	$n_y$	$\ n_y - n_{ye}\ _2 = 7.133143091353612 \times 10^{-4}$	3.90
	$n_z$	$\ n_z - n_{ze}\ _2 = 6.613351900551691 \times 10^{-4}$	4.02
256	$\phi$	$\ \phi - \phi_e\ _2 = 3.885536109260787 \times 10^{-4}$	3.98
	$n_x$	$\ n_x - n_{xe}\ _2 = 3.607710884265911 \times 10^{-5}$	3.88
	$n_y$	$\ n_y - n_{ye}\ _2 = 1.802250166619108 \times 10^{-4}$	3.96
	$n_z$	$\ n_z - n_{ze}\ _2 = 1.652681029440823 \times 10^{-4}$	4.00

Table 1: Convergence ratios  $R$  in an uniform grid  $n \times n \times n$  for the forced Model in the accuracy test problem ( $t = 10$ ).

## 5 NUMERICAL SIMULATIONS

Following [16] and [5], we take  $\lambda = 1.342 \times 10^{-2}$ ,  $\gamma = 4 \times 10^{-5}$ ,  $\delta = 6.25 \times 10^{-2}$ , and  $A = 6.708 \times 10^{-3}$ . To balance anchoring and elastic energy we select  $K = A$ . The relaxation time  $\tau$  is taken to be 1 and  $\varepsilon = \frac{4}{256}$ .

We consider spinodal decomposition starting from the slightly, randomly perturbed homogenous phase  $\phi \equiv 0$ . To this end, we take the initial order parameter  $\phi_0$  at each grid point  $(x_i, y_j)$  to be

$$\phi_0(x_i, y_j) = \xi_{ij},$$

where  $\xi_{ij} \in U(-\varepsilon, \varepsilon)$ , that is  $\xi_{ij}$  is a uniformly distributed random number in  $(-\varepsilon, \varepsilon)$ . The parameter  $\varepsilon$  is the same as that in the mixing energy (2), i.e. a measure of the interfacial thickness. The initial director field  $\mathbf{n}_0$  is given by  $\mathbf{n}_0(x_i, y_j, z_j) = \frac{(1, 1, \omega_{ij})}{\sqrt{2 + \omega_{ij}^2}}$  where  $\omega_{ij} \in U(-0.05, 0.05)$ . Figures 2 and 3 show spinodal decomposition with planar anchoring; Figures 4 and 5 show spinodal decomposition with homeotropic anchoring. It is possible to verify that the phase separation occurs very slowly and there is the formation of a coarsening pattern with a bicontinuous structure.



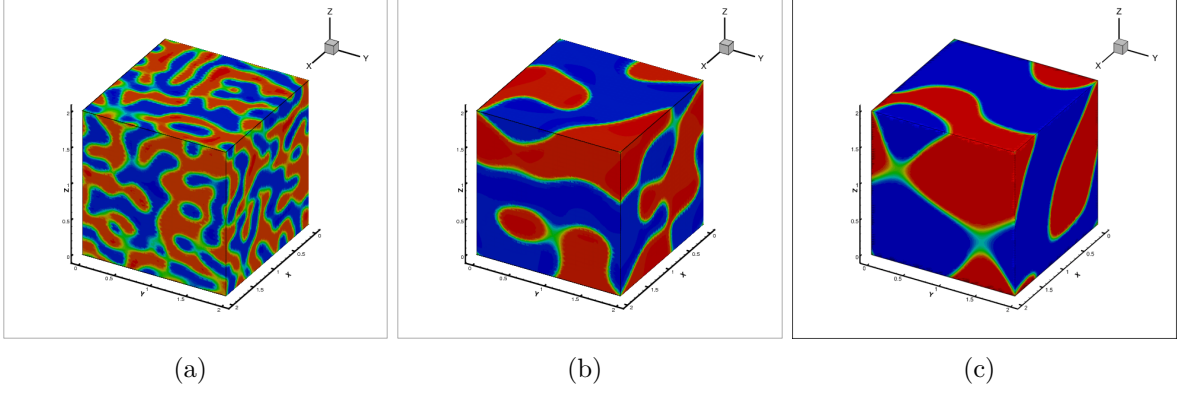


Figure 2: Spinodal decomposition with planar anchoring: contour in (a)  $t = 60$ , (b)  $t = 2050$  and (c)  $t = 9300$ .

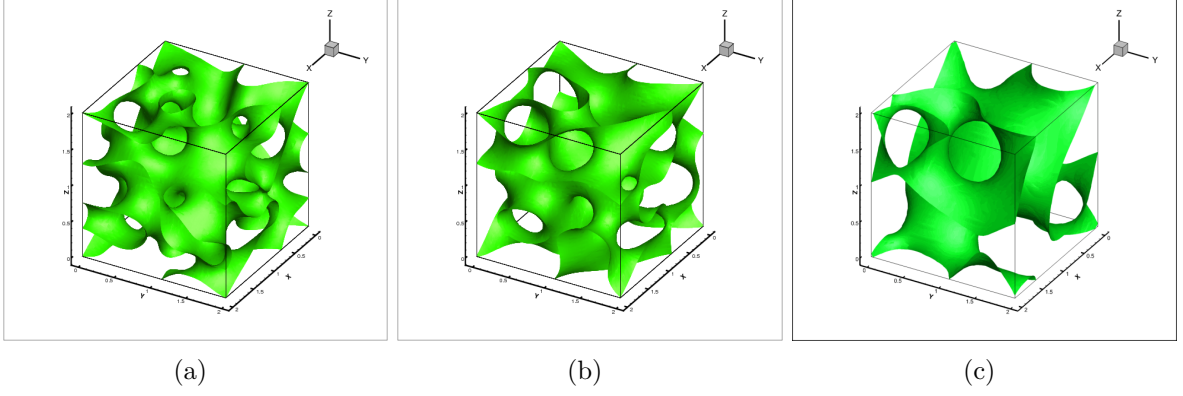


Figure 3: Spinodal decomposition with planar anchoring: isosurfaces ( $\phi = 0$ ) in (a)  $t = 1100$ , (b)  $t = 2050$  and (c)  $t = 9300$ .

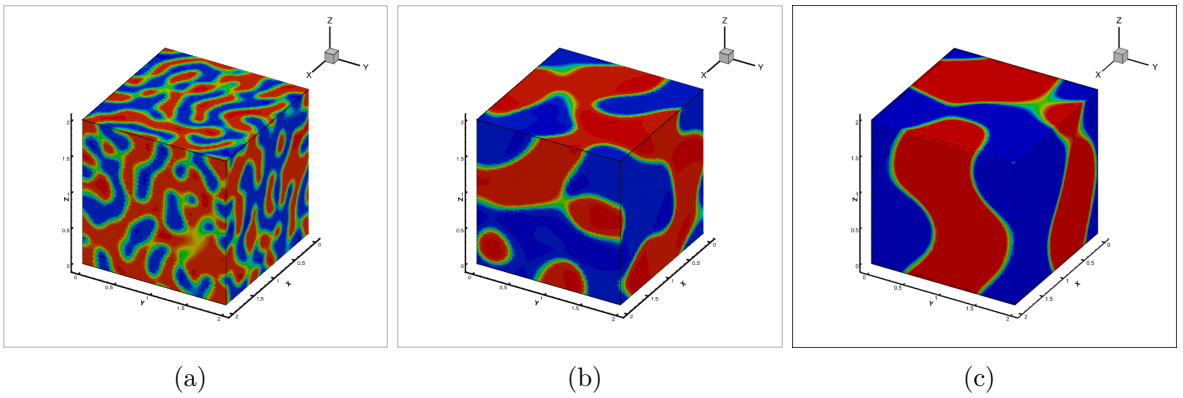


Figure 4: Spinodal decomposition with homeotropic anchoring: contour in (a)  $t = 60$ , (b)  $t = 2050$  and (c)  $t = 9300$ .

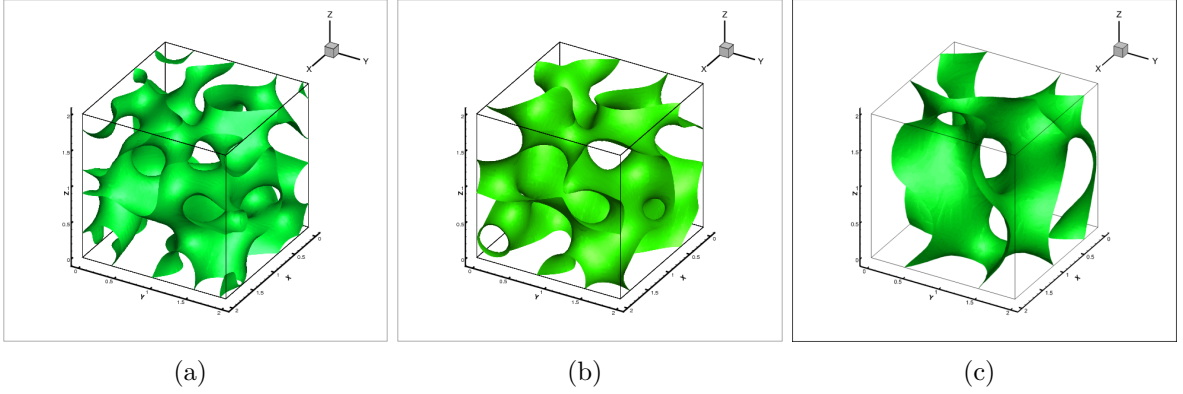


Figure 5: Spinodal decomposition with homeotropic anchoring: isosurfaces ( $\phi = 0$ ) in (a)  $t = 1050$ , (b)  $t = 2050$  and (c)  $t = 9300$ .

To simulate spinodal decomposition with nucleation, we take the initial condition

$$\phi_0(x_i, y_j) = 0.5 + \xi_{ij},$$

where  $\xi_{ij} \in U(-\varepsilon, \varepsilon)$ . This corresponds to a small random perturbation of the homogeneous state  $\phi \equiv 0.5$  where the liquid crystal is the dominant component. The initial director field is selected as before. Figures 6 and 7 show the spinodal decomposition with nucleation and homeotropic anchoring. It can be observed that the numerous drops defined by the initial condition coalesce forming a single large drop.

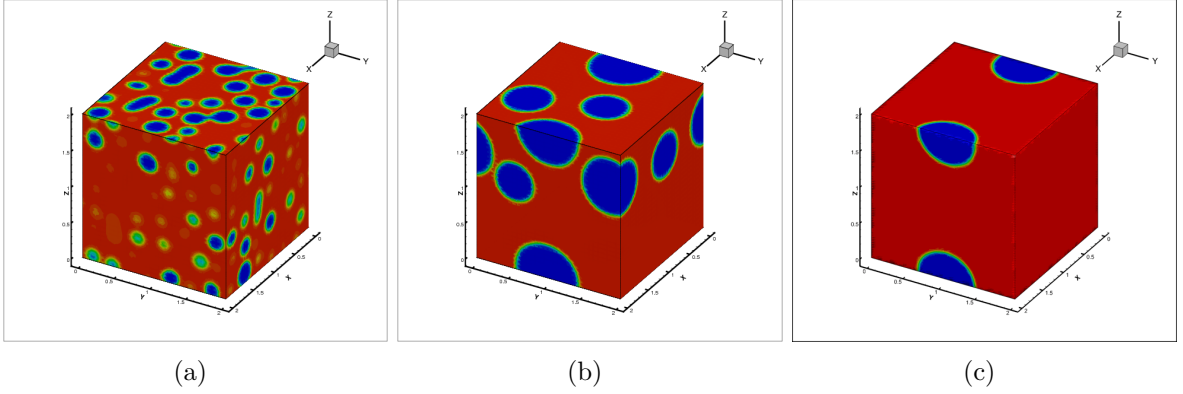


Figure 6: Spinodal decomposition with nucleation and homeotropic anchoring: contour in (a)  $t = 90$ , (b)  $t = 1400$  and (c)  $t = 7100$ .

Figures 8, 9 and 10 display the director field in the three cases of spinodal decomposition simulated.

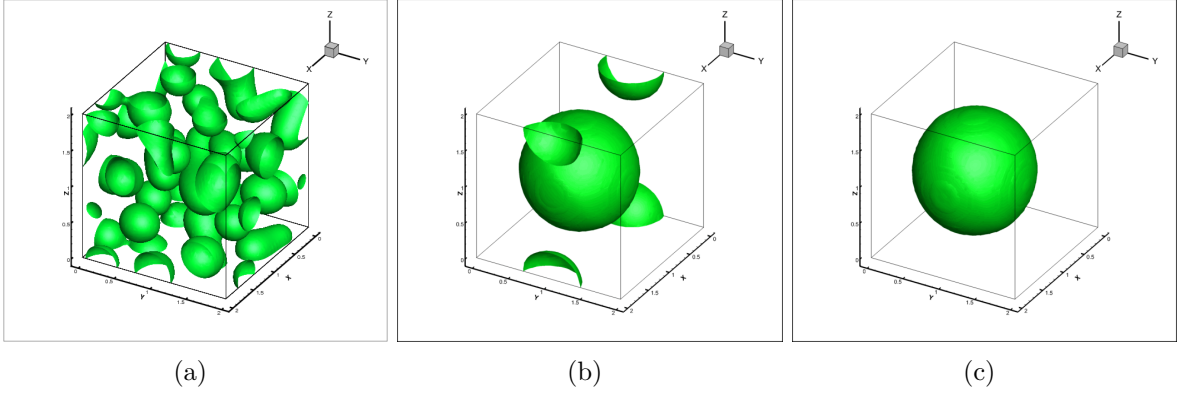


Figure 7: Spinodal decomposition with nucleation and homeotropic anchoring: isosurfaces ( $\phi = 0$ ) in (a)  $t = 450$ , (b)  $t = 7100$  and (c)  $t = 9200$ .

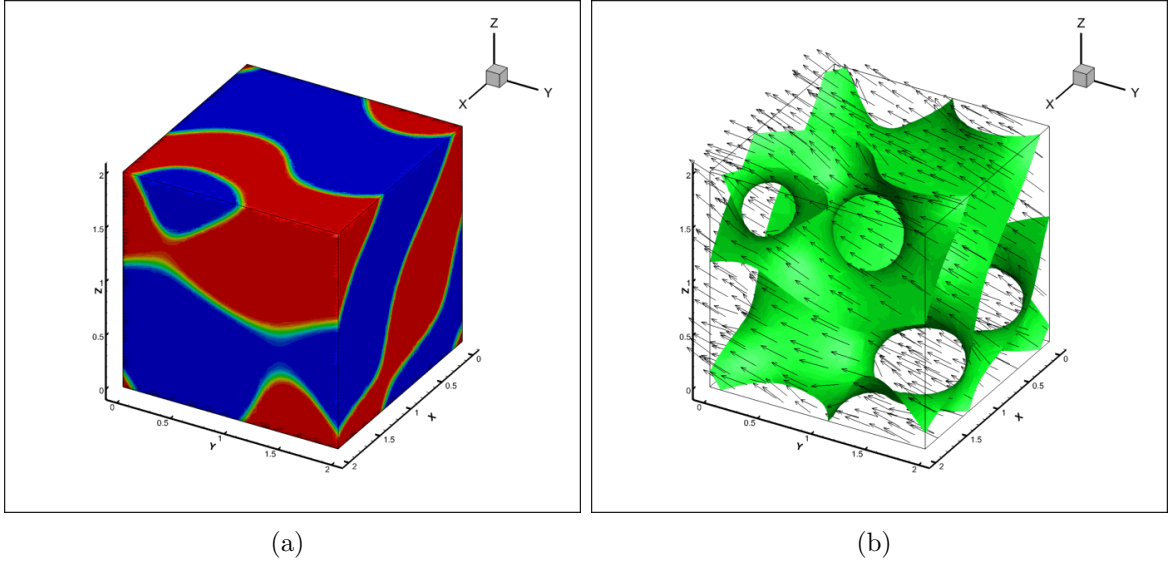


Figure 8: Spinodal decomposition with planar anchoring in  $t = 7300$ : (a) contour; (b) isosurfaces and director vector field.

## 6 CONCLUSIONS

The results presented in Section 5 are partial, since the simulations are still being performed. Our goal is to compare these results with the two-dimensional results obtained by Mata et al. [5]. As future work, we are interested in examining how these effects are modified in the presence of a flow, i.e. we intend to couple the equations of Model H with the equation of the director field.

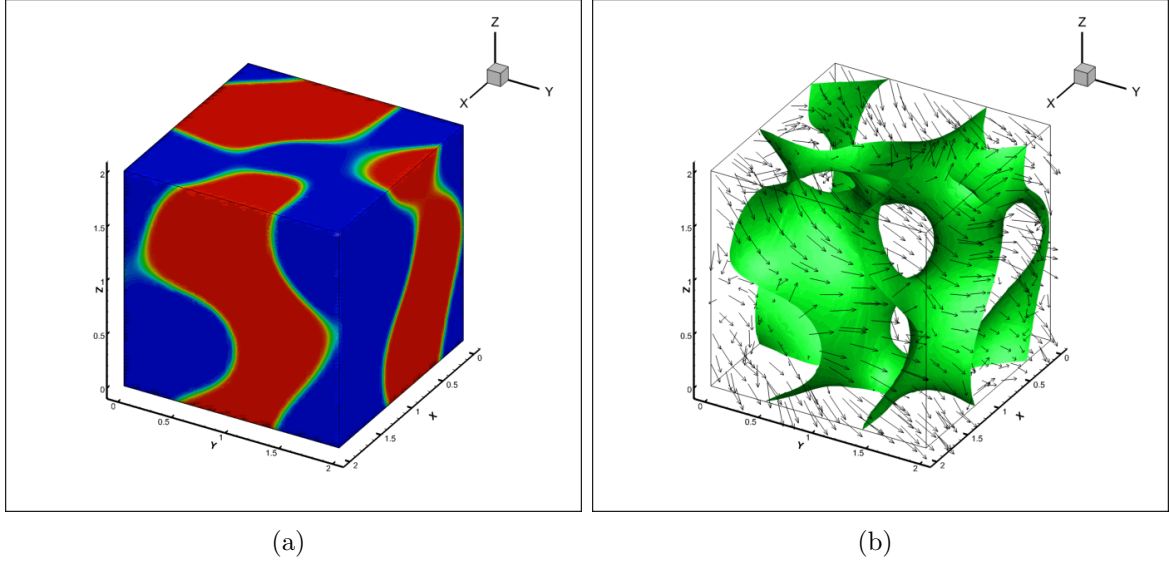


Figure 9: Spinodal decomposition with homeotropic anchoring in  $t = 7300$ : (a) contour; (b) isosurfaces and director vector field.

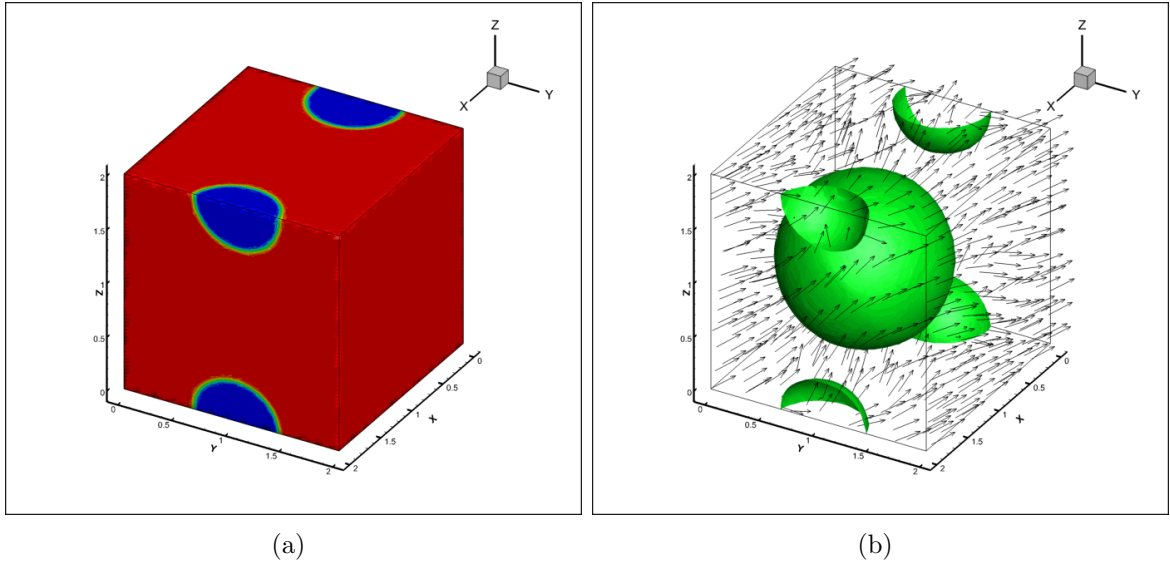


Figure 10: Spinodal decomposition with nucleation and homeotropic anchoring in  $t = 7100$ : (a) contour; (b) isosurfaces and director vector field.

## REFERENCES

- [1] R.L. Nos and A.M. Roma and H.D. Cenicerros, Solução de equações diferenciais parciais elípticas por técnicas multinível-multigrid em malhas tridimensionais bloco-estruturadas com refinamento localizado, *Anais do XXV Congresso Nacional de Matemática Aplicada e Computacional*, São Paulo (2005).

- [2] R.L. Nos, *Simulações de escoamentos tridimensionais bifásicos empregando métodos adaptativos e modelos de campo de fase*, Tese de Doutorado, Universidade de São Paulo, São Paulo (2007)
- [3] H.D. Ceniceros and R.L. Nos and A.M. Roma, Three-dimensional, fully adaptive simulations of phase-field fluid models, *J. Comput. Phys.*, Vol. **229**, n. **17**, pp. 6135–6155, (2010).
- [4] R.L. Nos and H.D. Ceniceros and A.M. Roma, Simulação tridimensional adaptativa da separação das fases de uma mistura bifásica usando a Equação de Cahn-Hilliard, *TEMA - Trends in Applied and Computational Mathematics*, Vol. **13**, n. **1**, pp. 37–50, (2012).
- [5] M. Mata and C.J. García-Cervera and H.D. Ceniceros, Ordering kinetics of a conserved binary mixture with a nematic liquid crystal component, *Journal of Non-Newtonian Fluid Mechanics*, Vol. **212**, pp. 18–27, (2014).
- [6] A.J. Bray, Theory of phase-ordering kinetics, *Advances in Physics*, Vol. **43**, n. **3**, pp. 357–459, (1994).
- [7] A.J. Bray, Coarsening dynamics of phase-separating systems, *Phil. Trans. R. Soc. Lond. A*, Vol. **361**, pp. 781–792, (2004).
- [8] M. Motoyama and H. Nakazawa and T. Ohta and T. Fujisawa and H. Nakada and M. Hayashi and M. Aizawa, Phase separation of liquid crystal-polymer mixtures, *Computational and Theoretical Polymer Science*, Vol. **10**, n. **3-4**, pp. 287–297, (2000).
- [9] J. Xia and J. Wang and Z. Lin and F. Qiu and Y. Yang, Phase separation kinetics of polymer dispersed liquid crystals confined between two parallel walls, *Macromolecules*, Vol. **39**, n. **6**, pp. 2247–2253, (2006).
- [10] Y.J. Jeon and Y. Bingzhu and J.T. Rhee and D.L. Cheung and M. Jamil, Application and new developments in polymer-dispersed liquid crystal simulation studies, *Macromolecular Theory and Simulations*, Vol. **16**, n. **7**, pp. 643–659, (2007).
- [11] A. Matsuyama and R. Hirashima, Phase separations in liquid crystal-colloid mixtures, *The Journal of Chemical Physics*, Vol. **128**, n. **4**, (2008).
- [12] S. Bronnikov and C. Racles and V. Cozan, Kinetics of the nematic phase growth across the isotropic-nematic phase transition in polymer-dispersed liquid crystals, *Liquid Crystals*, Vol. **36**, n. **3**, pp. 319–328, (2009).
- [13] S. Bronnikov and S. Kostromin and V.V. Zuev, Thermally induced isotropic-nematic phase separation in mixtures of low-molecular weight and polymer liquid crystals, *Soft Materials*, Vol. **11**, n. **1**, pp. 6–12, (2013).

- [14] R.L. Nos and H.D. Cenicerros and A.M. Roma, Three-dimensional simulations of a conserved binary mixture with a nematic liquid crystal and flexible polymer components, *IV Simpósio de Métodos Numéricos Computacionais da Universidade Federal do Paraná*, pp. 63–69, (2014).
- [15] P.C. Hohenberg and B.I. Halperin, Theory of dynamic critical phenomena, *Rev. Mod. Phys.*, Vol. **49**, n. **3**, pp. 435, (1977).
- [16] P. Yue and J.J. Feng and C. Liu and J. Shen, A diffuse-interface method for simulating two-phase flows of complex fluids, *J. Fluid Mech.*, Vol. **515**, pp. 293–317, (2004).
- [17] J.W. Cahn and J.E. Hilliard, Free energy of a nonuniform system I, *J. Chem. Phys.*, Vol. **28**, pp. 258, (1958).
- [18] J.W. Cahn and J.E. Hilliard, Free energy of a nonuniform system III, *J. Chem. Phys.*, Vol. **31**, pp. 688, (1959).
- [19] P.G. de Gennes and J. Prost, *The physics of liquid crystals*, Clarendon Press, (1993).
- [20] V.E. Badalassi and H.D. Cenicerros and S. Banerjee, Computation of multiphase systems with phase field models, *J. Comput. Phys.*, Vol. **190**, pp. 371–397, (2003).
- [21] H.D. Cenicerros and A.M. Roma, A nonstiff, adaptive, mesh refinement-based method for the Cahn-Hilliard equation, *J. Comput. Phys.*, Vol. **225**, n. **2**, pp. 1849–1862, (2007).